

# Characterization of “Free Base” and Metal Complex Thioalkyl Porphyrazines by Magnetic Circular Dichroism and TDDFT Calculations

Simone Ghidinelli, Sergio Abbate, Ernesto Santoro, Sandra Belviso,\* and Giovanna Longhi\*

Cite This: *J. Phys. Chem. B* 2021, 125, 264–280

Read Online

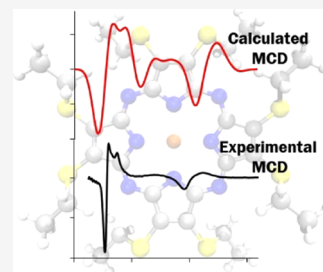
ACCESS |

Metrics &amp; More

Article Recommendations

Supporting Information

**ABSTRACT:** UV–vis absorption and magnetic circular dichroism (MCD) spectra of octakis thioethyl “free base” porphyrazine  $H_2OESPz$  and its metal complexes  $MOESPz$  ( $M = Mg, Zn, Ni, Pd, Cu$ ), as well as of  $[MnOESPz(SH)]$  were recorded. In the last case, MCD proved to have quite good sensitivity to the coordination of this complex with 1-methylimidazole (1-mim) in benzene. Time-dependent density functional theory (TDDFT) calculations were carried out for the considered porphyrazine complexes and showed good performance on comparing with MCD and UV–vis experimental spectra, even in the open-shell Cu and Mn cases. Calculations accounted for the red shift observed in the thioalkyl compounds and allowed us to reveal the role of sulfur atoms in spectroscopically relevant molecular orbitals and to highlight the importance of the conformations of the thioethyl external groups. Calculated MCD spectra of  $[MnOESPz(SH)]$  confirm the  $Mn(III) \rightarrow Mn(II)$  redox process, which leads to the  $[Mn(OESPz)(1-mim)_2]$  species, and the relevance of the spin state for MCD is revealed.



## INTRODUCTION

The highly delocalized  $\pi$ -electron system of tetrapyrrole macrocycles makes these systems ideal substrates for optoelectronics. In fact, porphyrins and phthalocyanines, the two most important subgroups of this family, find applications as dyes in organic photovoltaics (OPV)<sup>1,2</sup> and for the development of materials for nonlinear optics (NLO).<sup>3–6</sup> The structurally related porphyrazine macrocycles<sup>7–10</sup> have, however, been much less studied in this field, although they display interesting structural and optical properties. In fact, they allow ample and facile synthetic modularity, display a wider UV–vis absorption range, promising the development of panchromatic photovoltaic materials and, under some circumstances, can give rise to columnar liquid crystal mesophases.<sup>11–15</sup> Very few examples of porphyrazine applications in NLO<sup>16–24</sup> and OPV<sup>25,26</sup> have been reported, and only very recently some of us have described the potentiality of nonsymmetrically substituted thioalkyl porphyrazines in OPV<sup>27,28</sup> and NLO.<sup>29,30</sup> For the development of new optoelectronic materials based on the porphyrazine framework, a detailed knowledge of their electronic structure is of utmost importance. For this purpose, magnetic circular dichroism (MCD)<sup>31–37</sup> is quite a useful tool, displaying very attractive features with respect to standard UV–vis spectroscopy. In fact, MCD is more sensitive to the molecular electronic properties and, among others, offers the possibility of identifying degenerate excited electronic states because the resulting positive and negative bands make it possible to resolve overlapping electronic transitions. Such spectroscopy, also, often provides key information about the redox and spin state

of the central metal. The basis of the MCD theory was developed in the 1960–1970s.<sup>38,39</sup> A further key development of this technique has been provided by the recent application of density functional theory (DFT) computations for MCD spectra simulation;<sup>40–47</sup> correspondence between simulated and experimental spectra provides confidence in the picture obtained by simple time-dependent DFT (TDDFT) calculations, however, with due attention to possible TDDFT limitations, particularly in the case of open-shell systems.<sup>48,49</sup>

The MCD technique has been widely employed not only for investigating porphyrins' and phthalocyanines' electronic structures,<sup>32,33,50–53</sup> but also porphyrazine macrocycles<sup>53,54</sup> have been investigated; considering thioalkyl porphyrazines,<sup>55–58</sup> only a study by Stillman et al. is present in the literature<sup>59</sup> to the best of our knowledge. This prompted us to carry out an extensive MCD characterization on 2,3,7,8,12,13,17,18-octakis(ethylsulfanyl)-5,10,15,20-porphyrazine (OESPz) in its “free base” form  $H_2OESPz$ , its  $d^0$  Mg(II) complex, and a full series of transition-metal complexes:  $d^{10}$  Zn(II) and  $d^8$  Ni(II) and Pd(II) complexes, open-shell  $d^9$  Cu(II), and the  $d^7/d^6$  Mn(II)/Mn(III) redox couple (see Scheme 1).<sup>56</sup> TDDFT computations on selected examples offer deep insight into their electronic structure. It is

Received: October 13, 2020

Revised: November 29, 2020

Published: December 22, 2020



**Scheme 1. Structures of the Studied Compounds: “Free Base” H<sub>2</sub>OESPz, Octakis Thioethyl MOESPz Complexes, the Octakis Ethyl MgOEPz Complex, and Axially Coordinated Mn(II) and Mn(III) Complexes**

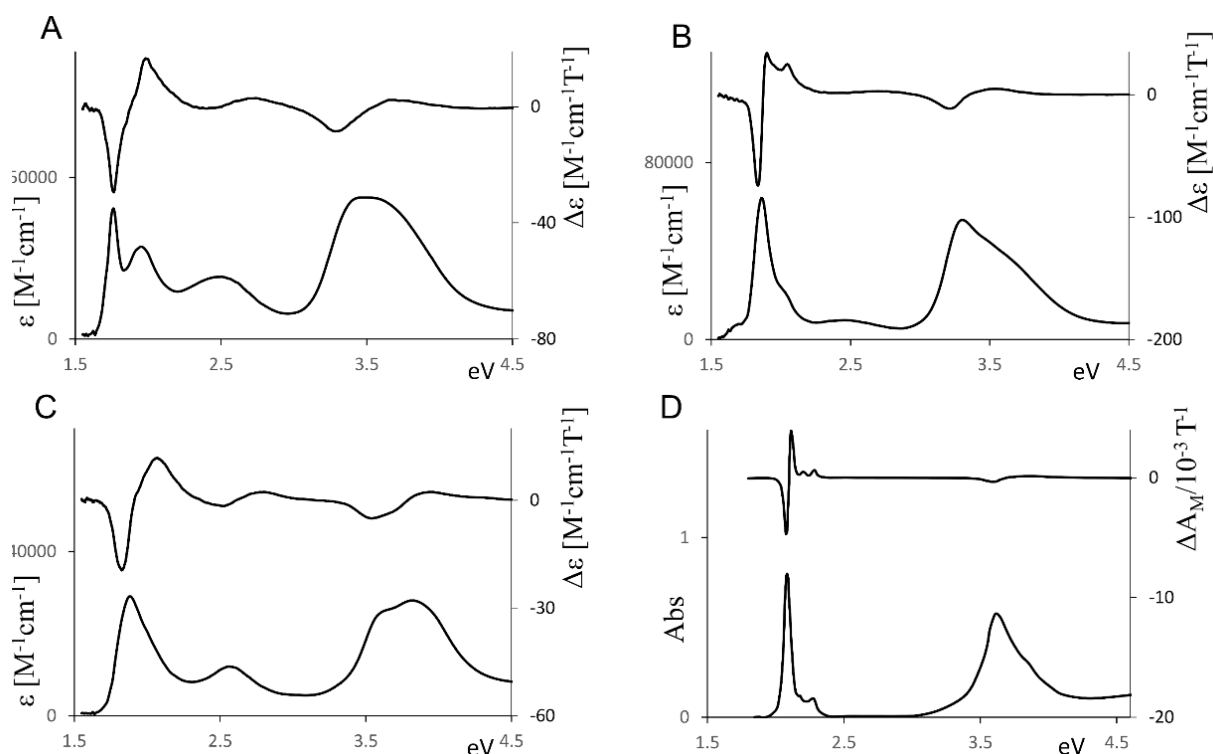
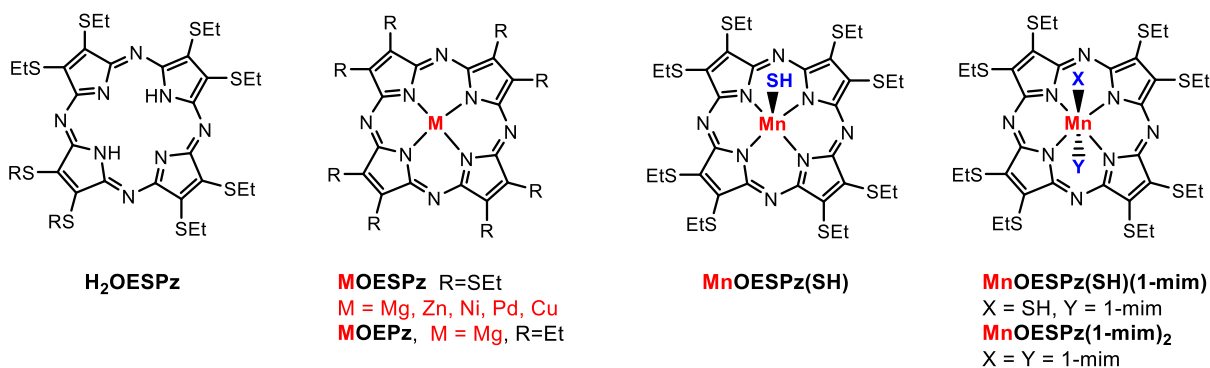


**Figure 1.** Experimental absorption and MCD spectra of “free base” thioethyl porphyrazine H<sub>2</sub>OESPz (A), MgOESPz (B) and NiOESPz (C) thioethyl porphyrazine complexes, and Mg ethylporphyrazine MgOEPz (D); the last data have been redrawn from ref 59.

worthwhile to recall that the Mn(II) thioethyl porphyrazine complex has been reported to possess interesting catalytic properties affording easy removal of halogen atoms from halogenated hydrocarbons via oxidative addition to manganese.<sup>55–58</sup> This allows even defluorination of organic halides, proceeding through activation of the scarcely reactive C–F bond, thus paving the way to environmental applications for dehalogenation of dangerous organic pollutants.<sup>56</sup> Such a dehalogenation process occurs through an interconversion of the Mn(II)/Mn(III) redox couple, which was investigated through absorption spectroscopy, since the two species have different typical UV–vis spectral features.<sup>56</sup> The same redox process is investigated here by MCD spectroscopy, which may, in principle, guarantee a higher sensitivity and selectivity than UV–vis absorption analysis. In fact, even if the MCD signal arises from the same transitions as those determining the UV–visible absorption spectrum, the selection rules are different. Moreover, the presence of positive/negative features permits

us to better resolve different adjacent almost degenerate transitions such that the correspondence theory–experiment is for sure more stringent.

## EXPERIMENTAL SECTION

**General Procedures.** All chemicals and solvents (Aldrich) were of reagent grade. Solvents were dried and distilled before use according to standard procedures.

**Synthesis.** Compounds H<sub>2</sub>OESPz,<sup>11–15,60,61</sup> MgOESPz,<sup>11,12,62</sup> ZnOESPz,<sup>11</sup> NiOESPz,<sup>11–15</sup> PdOESPz,<sup>28</sup> CuOESPz,<sup>11–15,62</sup> and [(MnOESPz)(SH)]<sup>55,56</sup> were prepared following previously reported procedures. Their spectroscopic data matched those reported here.

**Spectroscopic Measurements.** UV–vis and MCD spectra were recorded in the 250–800 nm range using a J-815SE spectrometer, with a home-built cell holder equipped with a 0.6 T permanent magnet, in 1-cm pathlength quartz cells (the concentration of the solutions was ca. 10<sup>–5</sup>–10<sup>–6</sup> M)

at room temperature, 200 nm/min scanning speed, and 10 scans per measurement. For each sample, the two magnetic field orientations were tested and enantiomericity of the two magnetic field directions was checked.

**Computational Methods.** Calculations were performed with ADF program 2018.105.<sup>63,64</sup> The BP86 functional combined with Grimme's D3 correction<sup>65</sup> and the TZP basis set was employed for structure optimization. Excitation energies, oscillator strengths, and MCD parameters<sup>40–42,66</sup> were computed by TDDFT formalism using the M06-L functional and TZP basis set. Molecular orbitals were generated by Molden software.<sup>67</sup> For open-shell compounds (copper and manganese complexes), the spin-unrestricted formalism was employed using the same functional and basis set used for the closed-shell molecules. Scalar ZORA<sup>68,69</sup> approximation was used for the relativistic effects. Electronic excitation energies were found with the Davidson procedure for open-shell systems in a spin-unrestricted TDDFT calculation with scalar ZORA and no frozen core.

## RESULTS AND DISCUSSION

**Absorption and MCD Spectra.** Porphyrazines MOESPz were prepared as already described in refs 11 and 55–58.

UV–vis and MCD spectra have been recorded in dichloromethane (DCM) in the 250–800 nm range. We report in Figure 1, the spectra of H<sub>2</sub>OESPz, NiOESPz, MgOESPz and, for comparison and discussion, absorption and MCD spectra of an analogous alkyl-substituted Mg complex, which is Mg-octaethyltetraazaporphyrin MgOEPz, taken from ref 59.

**“Free Base” H<sub>2</sub>OESPz.** All UV–vis spectra exhibit the typical features of nonaggregate thioalkyl porphyrazines; for the “free base”, the two Q<sub>x</sub> and Q<sub>y</sub> bands can be easily distinguished at 1.77 eV (704 nm) and at 1.94 eV (635 nm), respectively; the Soret band is observed at about 3.53 eV (357 nm), and its shape suggests contributions from two bands at about 3.43 (361 nm) and 3.58 eV (346 nm). Both the Q and B features are red-shifted with respect to alkyl-substituted porphyrazines. Furthermore, as typical of the thioethyl porphyrazine, there is an intermediate broad, less intense, “extra” band between the Q and B features, at about 2.53 eV (495 nm). This feature (in ref 70 called the W band) in early studies had been associated with a  $n_{\text{sulfur}} \rightarrow \pi^*$  transition,<sup>29,70,71</sup> and, more recently, based on calculations, was attributed to a shifted B component<sup>72</sup> of the Soret band.<sup>73</sup> The MCD spectra are similar but not identical for all examined compounds as we are going to comment below. Considering H<sub>2</sub>OESPz, only Faraday B-terms are expected, in accordance with the other D<sub>2h</sub> symmetry (or lower) metal-free tetrapyrroles.<sup>37,74</sup> In fact, two B-terms are associated with the Q<sub>x</sub> and Q<sub>y</sub> transitions, with a negative band at 1.76 eV (705 nm) and a positive one at 2 eV (622 nm). The sign of the Q doublet is related<sup>34,35</sup> to the energy difference between the first two excited states, which is lower than the energy difference between the two occupied states involved in the dipole allowed transitions ( $\Delta\text{LUMO} < \Delta\text{HOMO}$  considering Gouterman orbitals<sup>75</sup>). Analogously a (–, +) doublet is observed in correspondence to the UV Soret band with the negative band at 3.3 eV (377 nm) and the positive one at 3.64 eV (339 nm). Such spectral features closely resemble those displayed by tetra-*tert*-butyl porphyrazine.<sup>52</sup> The MCD spectrum of H<sub>2</sub>OESPz also displays a positive band at 2.7 eV (461 nm), which does not exactly correspond to the UV–vis “extra” band located at a longer wavelength. All assignments will be

discussed in the following, based on the results of TDDFT calculations.

**Metal Complexes.** Metal complexes of symmetrically substituted porphyrazines present a D<sub>4h</sub> symmetry core, if one disregards possible distortions from the planarity of the core itself or the pendant conformational degree of freedom (see the following Results and Discussion); therefore, in their MCD spectra Faraday A-term features are expected in correspondence to the main UV–vis absorption bands.<sup>34–37</sup> Due to the higher molecular symmetry, the UV–vis spectra of the porphyrazine metal complexes MOESPz display a single Q band, which is blue-shifted (ca. 40–45 nm = 0.10–0.11 eV) compared to that of the corresponding “free base”. In fact, the MCD spectra of the investigated metal complexes present the typical features whose assignment can be based on the Gouterman four-orbital scheme<sup>75</sup> or the Michl perimeter model<sup>76</sup> based on the electronic description by Moffitt<sup>77</sup> and Michl;<sup>34</sup> these electronic models account for the most intense features observed for all porphyrinoids. Based on these schemes, the lowest unoccupied levels are 2-fold degenerate  $\pi^*$  orbitals, thus justifying the presence of A-terms; in the case of porphyrins, the highest energy occupied levels are  $\pi$  orbitals a<sub>2u</sub> and a<sub>1u</sub> for D<sub>4h</sub> symmetry; these states are nearly degenerate in the case of porphyrin, while are well separated in energy in porphyrazines.<sup>53,78,79</sup> In fact, in the latter case the presence of electronegative nitrogen atoms in the meso position lowers the energy of a<sub>2u</sub> states with respect to that of a<sub>1u</sub> states.<sup>53</sup> This fact allows mixing of the forbidden Q transitions and allowed B transitions, which results in the intensification of the Q band. In general, calculations indicate that the metal center has only a minor influence on the energy values of both the higher occupied and lower unoccupied orbitals for porphyrazine metal complexes.<sup>53</sup> MCD spectra of d<sup>0</sup> Mg(II) and d<sup>10</sup> Zn(II) complexes appear almost superimposable (see Figure S1 in the Supporting Information (SI)) but also the d<sup>9</sup> Cu(II) complex shows a similar Q feature. In particular, the MCD spectral shape of the Mg(II) complex (Figure 1B) suggests the presence of an intense Faraday A-term feature centered at about 1.87 eV (664 nm), in correspondence to the UV–vis maximum of the Q band at 1.85 eV (671 nm); however, such a spectral feature is nonsymmetrical, and its positive higher energy branch partly overlaps with other A- and/or B-terms allied to the feature at 2.36 eV (609 nm, precise assignment will be discussed in the following). Finally, a weaker Faraday A-term centered at 3.41 eV (364 nm) is associated with the UV–vis Soret broad feature at 3.81–3.54 eV (325–350 nm).

The Ni(II) and Pd(II) OESPz complexes display very similar UV–vis and MCD spectra (Figure S2 in the SI), which are also similar to those for the “free base”, especially considering the Q region, but are quite different from those of the Mg, Zn, and Cu complexes. The experimental MCD spectrum of the d<sup>8</sup> Ni complex shows (Figure 1C) an asymmetric positive Faraday A-term centered at 1.91 eV (650 nm), in correspondence to the maximum of the Q band at the same wavelength; the origin of this asymmetry needs calculations for a correct assignment. In correspondence to the broad Soret band located at around 3.54 eV (350 nm), a positive A-term is expected and is indeed observed, again presenting broadness and asymmetry. Finally, a positive MCD feature centered at 2.58 eV (480 nm), approximately in correspondence to the “extra” band absorption at 2.56 eV (484 nm) is observed.



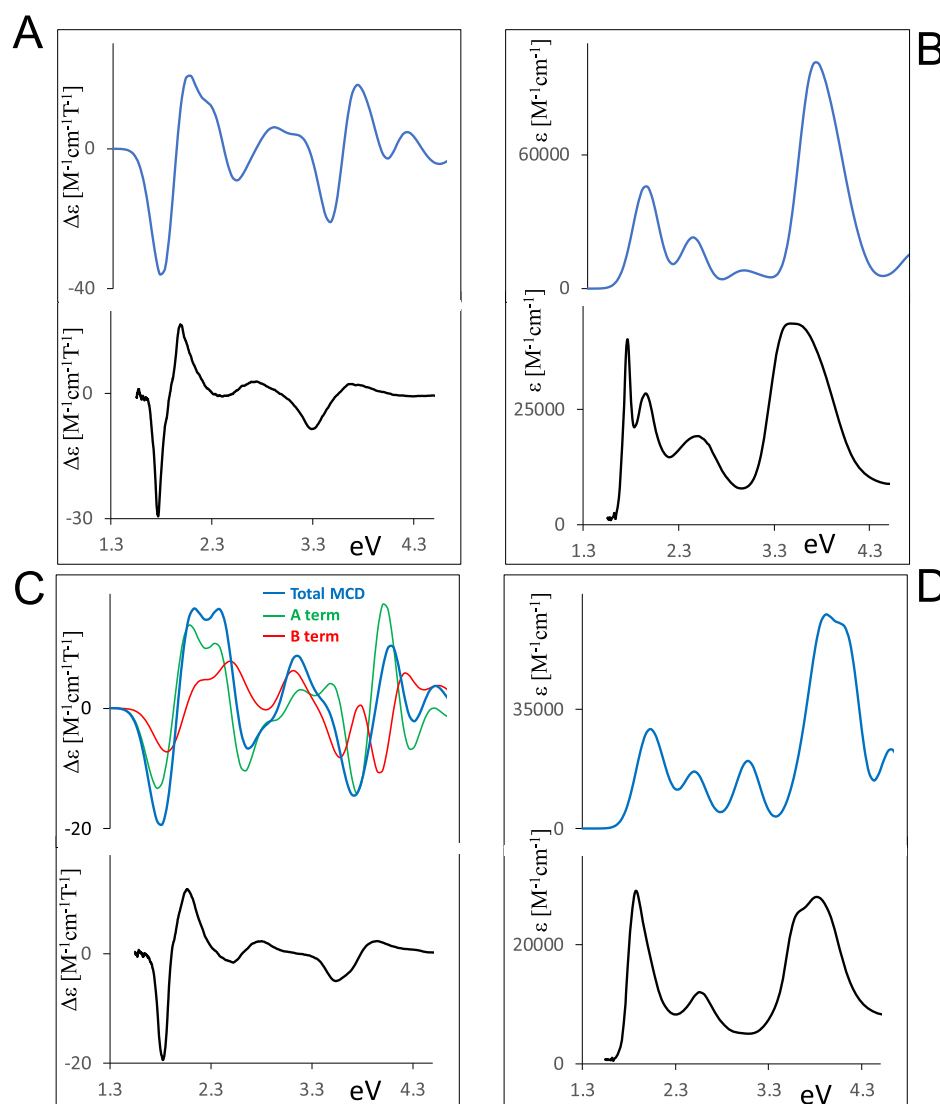


**Figure 3.** Comparison of experimental (black lines) and calculated (colored lines) UV–vis and MCD spectra. (A) Calculated and experimental MCD spectra of  $\text{H}_2\text{OESPz}$ . (B) Calculated and experimental UV–vis spectra of  $\text{H}_2\text{OESPz}$ . (C) Calculated and experimental MCD spectra of  $\text{NiOESPz}$ . (D) Calculated and experimental UV–vis spectra of  $\text{NiOESPz}$ .

conformers in solution. For this reason, comparison with a different symmetry pattern (*udud*), that is the most commonly studied  $D_2$  (free base) and  $D_4$  (four coordinated metal complexes), will be presented below.

**Energy Levels and Orbitals.** We report in Figure 2, the calculated energy levels of the four significant cases corresponding to the experimental data presented in Figure 1: the “free base”, Ni metal complex, Mg metal complex, and the alkyl-substituted MgOEPz complex. The relevant molecular orbitals are presented in Figure S3A,B. The lowest unoccupied molecular orbital (LUMO) (corresponding to the Gouterman LUMO orbital) presents similar energies and similar atomic contributions in the three thioalkyl compounds. In the case of the free base, the two orbitals 53b1 and 53b2 are nearly degenerate and similar to 56e and 54e of Ni and Mg complexes, respectively; they are all similar in shape and atomic contribution to the degenerate state 38e1 of the MgOEPz, which, however, is found at a higher energy. Similarly, the first occupied orbitals of the Gouterman type (responsible for the Q bands) are similar in the four cases (48a2, 26b1, 25b1, and 17b1); however, the thiolate

compounds show important contributions from sulfur atoms. The energy value is quite similar for the three thiolate compounds, while it is slightly higher in the case of MgOEPz, so that the optical gap corresponding to the first optical transition is expected at a lower energy in the thio-compounds, as in fact observed. The lower energy Gouterman orbitals (55a1, 29b2, 28b2, and 20b2) involved in the B transitions are very similar in the four cases since sulfur atoms are only marginally involved, while a large contribution originates from nitrogen atoms, as expected; since this orbital is localized within the macrocycle, it is similar to that calculated for the MgOEPz complex (see Figure S3B). The corresponding energy level displays some slight differences in the considered complexes; in the presence of nickel, the energy is lower as compared to the metal-free case or the MgOESPz complex; in the case of MgOEPz, one calculates a higher energy but the difference is not as pronounced as that for the highest occupied molecular orbital (HOMO) case. This explains why the blue shift of the Soret band of MgOEPz is lower than what was observed for the Q band. In Figure S3A,B other orbitals involved in optically active transitions are reported and most of

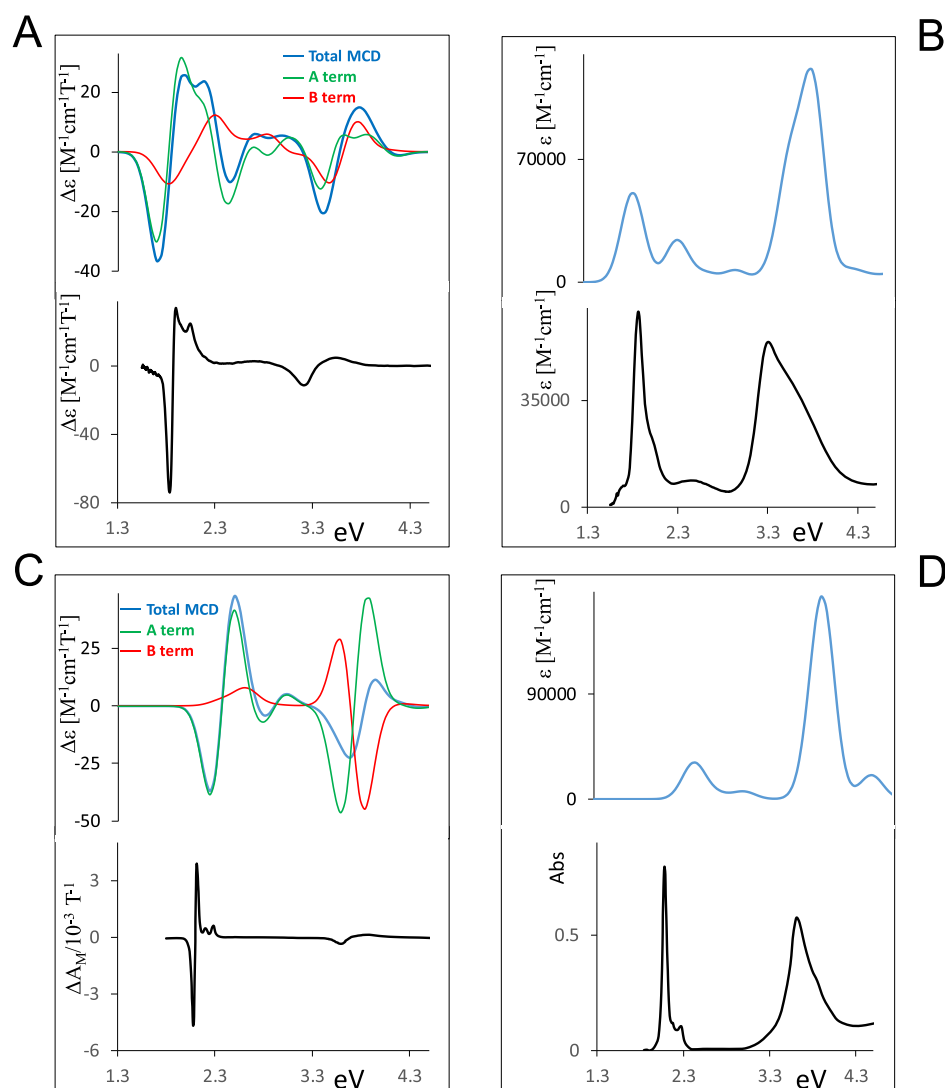


**Figure 4.** Comparison of experimental (black lines) and calculated (colored lines) UV–vis and MCD spectra. (A) Calculated and experimental MCD spectra of MgOESPz. (B) Calculated and experimental UV–vis spectra of MgOESPz. (C) Calculated and experimental MCD spectra of MgOEPz. (D) Calculated and experimental UV–vis spectra of MgOEPz.

them show large contributions from sulfur atoms. Among the metal orbitals, in the energy range of the observed bands, one can recognize the nickel orbitals (occupied 32a1, unoccupied 31b2), while the corresponding ones for Mg are not in the range of interest.

**Calculated Spectra.** From the performed calculations, it is possible to evaluate the spectroscopic response also. A comparison of experimental and calculated spectra is given in Figure 3 for the “free base” and for NiOESPz and in Figure 4 for MgOESPz and MgOEPz. The correspondence is not perfect, but acceptable, and allows us to recognize and to assign the various features, as reported in Table 1.

The two  $Q_x$  and  $Q_y$  components observed for the metal-free compound can be assigned to transitions from 48a2, the HOMO Gouterman orbital bearing high contributions from sulfur atoms to LUMO and LUMO + 1 states. They possess similar oscillator strengths and two B-terms, the lowest energy one negative and the second positive, as expected, since the two HOMO, HOMO – 1 Gouterman states present an energy difference value larger than that for LUMO, LUMO + 1.<sup>34,35</sup> The intense B band receives contributions from three main

transitions evidenced in Table 1A, involving the pure Gouterman type orbital 55a1 only partially and also presenting consistent contributions from orbitals of the same symmetry but involving sulfur atoms, like 54a1. As already observed, absorption and MCD features are also recorded and calculated at intermediate energies between the Q and B regions. The main absorption contributions at about 2.35 eV (528 nm) involve the occupied orbital 47a2 localized on sulfur atoms and present B-terms of the opposite sign, partially canceling out due to near-degeneracy. The positive MCD feature observed at about 2.85 eV (435 nm) is calculated as the convoluted sum of many transitions between 2.73 and 3.07 eV (454, 404 nm), with contribution from orbitals quite delocalized on the azaporphyrin core and on the sulfur pendant groups and also with some contribution from the Gouterman orbital 55a1. It should be noted, however, that the features calculated in this intermediate range are highly dependent on the pendant groups’ conformation (which also dictates different symmetries). A comparison with the spectra calculated for the  $D_2$  *udud* conformation is shown in Figure S4.

Table 1. Principal Calculated Transitions Accounting for the Observed Bands: Wavelength (nm), Energy (eV), Oscillator Strength (f), Magnetic Terms A (au) and B (au), Symmetry, and Wavefunctions<sup>a</sup>

A							H <sub>2</sub> OESPz			
nm	eV	f	$\mathcal{E}$				wavefunction			
671	1.85	0.22	-3864.5	B1	Qx		48a2→53b2(0.48)	56a1→53b1(0.37)		
651	1.90	0.29	3581.5	B2	Qy		48a2→53b1(0.59)	56a1→53b2(0.31)		
528	2.35	0.21	4724.4	B1			47a2→53b2			
525	2.36	0.04	-4414.9	B2			47a2→53b1			
453	2.74	0.00	-134.0	B1			46a2→53b2			
445	2.79	0.03	170.9	B2			46a2→53b1(0.77)	45a2→53b1(0.12)		
436	2.84	0.04	64.4	B1			52b2→49a2			
422	2.94	0.01	-66.0	B2			45a2→53b1(0.71)	55a1→53b2(0.23)		
409	3.03	0.01	-148.7	B2			54a1→53b2(0.54)	55a1→53b2(0.31)		
404	3.07	0.02	219.6	B1			54a1→53b1(0.46)	55a1→53b1(0.42)		
358	3.46	0.33	-819.1	B2	B MCD<0		51b1→49a2(0.62)	54a1→53b2(0.17)	55a1→53b2(0.12)	
350	3.55	0.60	107.1	B1	B		54a1→53b1(0.32)	53a1→53b1(0.19)	51b2→49a2(0.17)	55a1→53b1(0.17)
346	3.59	0.04	1021.7	B2	MCD>0		53a1→53b2			
336	3.69	0.06	-1144.3	B1	MCD<0		53a1→53b1			
333	3.73	0.44	807.1	B2	B MCD>0		53a1→53b2(0.25)	51b1→49a2(0.20)	54a1→53b2(0.18)	55a1→53b2(0.16)
324	3.83	0.13	309.4	B1			51b2→49a2			
315	3.93	0.10	-907.1	B2			52a1→53b2			
312	3.98	0.07	614.1	B1			52a1→53b1			

B							NiOESPz		
nm	eV	f	$\mathcal{A}$	$\mathcal{E}$			wavefunction		
678	1.83	0.14	2.16	-229.0	E	Q	26b1→56e(0.68)	30b2→56e(0.18)	
632	1.96	0.25	2.72	-81.8	E		30b2→56e(0.63)	26b1→56e(0.17)	
610	2.03	0.00	-0.03	-33.3	E		32a1→56e		
587	2.11	0.12	0.19	194.0	E		55e→31b2		
505	2.45	0.18	-2.02	216.6	E		23a2→56e		
453	2.74	0.02	0.19	-7.0	E		25b1→56e(0.68)	24b1→56e(0.19)	
423	2.93	0.01	0.08	-130.0	E		24b1→56e(0.60)	55e→24a2(0.19)	
412	3.01	0.21	0.46	263.0	E		55e→24a2(0.74)	24b1→56e(0.11)	
366	3.39	0.01	0.03	17.7	E		53e→31b2		
349	3.56	0.05	-0.69	-455.5	E		31a1→56e(0.84)	54e→24a2(0.12)	
344	3.60	0.04	0.00	291.4	E		54e→24a2(0.82)	31a1→56e(0.14)	
329	3.77	0.25	1.10	334.0	E	B	29b2→56e(0.38)	28b2→56e(0.26)	53e→24a2(0.14)
323	3.84	0.02	0.15	-435.3	E		28b2→56e(0.62)	52e→31b2(0.23)	
317	3.91	0.03	0.14	-108.8	E		23b1→56e(0.37)	53e→24a2(0.28)	52e→31b2(0.26)
307	4.04	0.52	-1.06	243.0	E	B	53e→24a2(0.43)	29b2→56e(0.24)	

Table 1. continued

C						MgOESPz	
nm	eV	f	$\mathcal{A}$	$\mathcal{B}$			wavefunction
679	1.83	0.55	8.62	-408.7	E	Q	25b1 → 54e (0.75) 29b2 → 54e (0.13)
542	2.29	0.26	0.00	3.6	B2		52e → 54e
539	2.30	0.26	-3.17	360.0	E		23a2 → 54e
476	2.61	0.06	0.82	84.7	E		24b1 → 54e
424	2.92	0.03	0.06	1355.3	E		53e → 24a2 (0.81) 23b1 → 24a2 (0.14)
423	2.93	0.04	0.57	-1243.3	E		23b1 → 54e (0.65) 28b2 → 54e (0.15)
421	2.94	0.02	0.00	-4.4	B2		25b1 → 24a2
397	3.12	0.00	0.00	4.7	B2		51e → 54e
379	3.27	0.01	0.07	-49.9	E		27b2 → 54e (0.79) 28b2 → 54e (0.16)
376	3.30	0.05	-0.47	44.6	E		30a1 → 54e
353	3.51	0.70	1.47	-233.5	E		52e → 24a2
330	3.76	1.21	0.56	209.9	E	B	28b2 → 54e
316	3.92	0.00	0.00	-4.4	B2		24b1 → 24a2
305	4.07	0.02	-0.19	11.4	E		29a1 → 54e

D						MgOEPz	
nm	eV	f	$\mathcal{A}$	$\mathcal{B}$			wavefunction
522	2.38	0.33	8.46	72.8	E	Q	17b1 → 38e
473	2.62	0.05	-0.62	195.4	E		23a1 → 38e
454	2.73	0.00	0.00	0.4	B2		37e → 38e
432	2.87	0.00	0.01	-0.8	E		16b1 → 38e
425	2.92	0.07	0.88	11.9	E		21b2 → 38e
367	3.38	0.00	0.00	4.3	B2		36e → 38e
343	3.61	0.00	0.00	-4.6	B2		17b1 → 16a2
338	3.67	0.46	3.05	1255.0	E		19b2 → 38e (0.73) 20b2 → 38e (0.22)
328	3.78	1.55	4.80	-1464.3	E	B	20b2 → 38e (0.56) 19b2 → 38e (0.27)
296	4.19	0.00	-0.03	8.1	E		22a1 → 38e
289	4.29	0.22	-0.09	8.2	E		37e → 16a2

<sup>a</sup>Occupied Gouterman orbitals are written in red.

The absorption and MCD spectra of the nickel complex are similar to those of the “free base”. From the results of the calculations in Table 1B, one may see that the first two transitions are separated by only 0.13 eV (45 nm), and present two positive A-terms giving rise to a spectral shape similar to the first set of four transitions for the “free base”, for which they exhibit a large oscillator strength and a sequence of (-,+)(-,+) B-terms. In the nickel case, however, the long positive tail bears contribution from a transition calculated at 2.45 eV (506 nm) with the negative A-term; in this case the positive low-energy contribution sums up with the higher energy positive contribution of the positive A-term of the previous transition. B-terms are present but show minor relevance. The nickel (32a1) → LUMO metal to ligand transition has a negligible oscillator strength and MCD activity. The intense B band receives contributions from the two main transitions evidenced

in Table 1B, partially involving the Gouterman type orbital 29b2 and presenting consistent contributions also from sulfur atoms (53e → LUMO + 1 in the case of the second intense transition); these two transitions show a positive and a negative A-term, respectively. However, also B-terms are to be considered in this region, as illustrated in Figure 3C. It should be noted that in the presence of Ni, the B band is blue-shifted when compared with the MgOESPz complex or metal-free H<sub>2</sub>OESPz and the same is observed with the Cu metal complex. Absorption and MCD features are present in between the Q and B regions and in this case, the contribution of B-terms appears responsible for the MCD activity.

Similar comments/assignments can be made for MgOESPz (Figure 4). The MCD spectrum is characterized by a doublet with a peculiar shape, which can be assigned to an A-term involving Gouterman orbitals with a non-negligible negative B

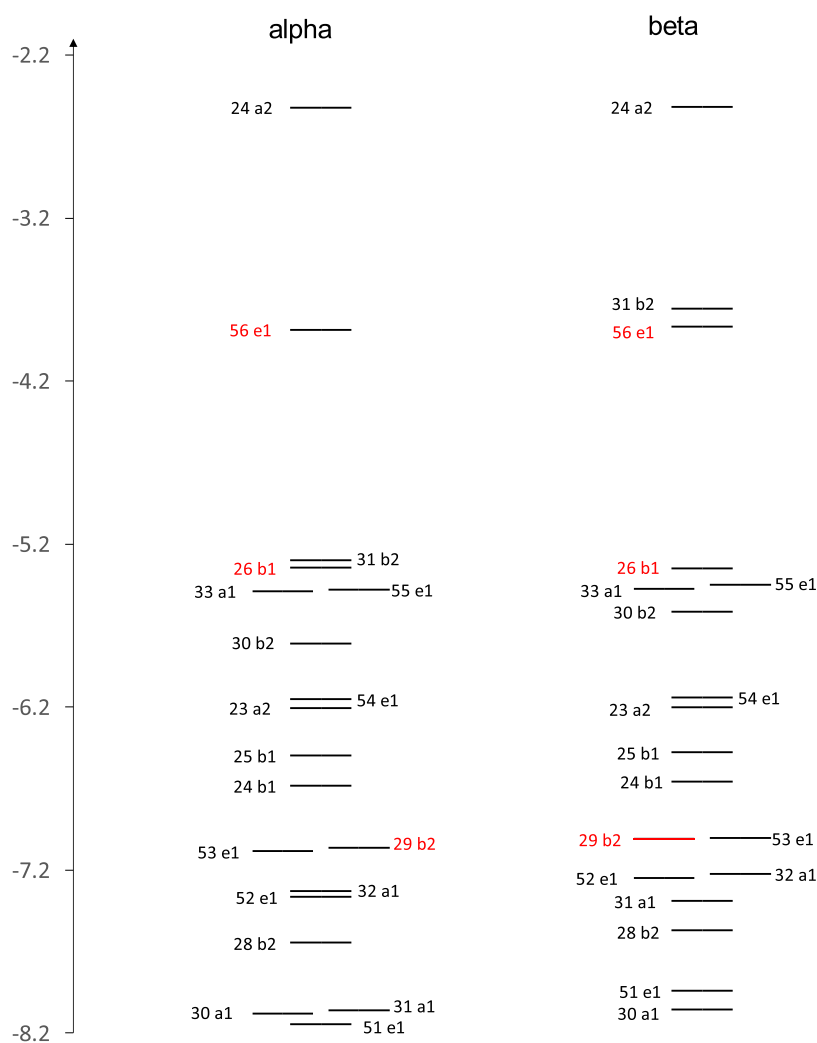


**Figure 5.** Calculated energy levels CuOESPz (Gouterman orbitals written in red).

contribution, followed by a second transition with an initial state 52e localized on sulfur atoms, with a smaller oscillator strength, opposite A-term, and opposite B term (Table 1C).

The intermediate spectroscopic region corresponds to absorption with quite a low oscillator strength and MCD activity; two degenerate intense B-terms of opposite signs nearly cancel each other. The B band presents two components; the one with a larger oscillator strength, at higher energy, can be assigned to the classical Gouterman orbital 28b2, while the one bearing the largest MCD activity is due to a positive A-term again involving sulfur contributions of the initial state 52e and the excited state 24a1. Considering the band assignment for the three cases just examined, we can say that the configuration interaction evidenced a complex pattern underneath the high-energy B features and the weak “extra” band W; the classical HOMO – 1 Gouterman orbital is well localized on the macrocycle nitrogen atoms, even though it contributes to the B band together with orbitals localized on sulfur atoms; orbitals with different symmetries contribute to the “extra” band transitions with just a weak involvement of the HOMO – 1 orbital. Through the same type of calculations, energy levels, wavefunctions based on eigenvectors predicted by the TDDFT method, absorption, and MCD spectra of the octaethyl Mg porphyrine complex can be obtained, and the findings are very similar to the other literature studies on

porphyrines. MgOEPz presents few sharp bands calling for a much simpler picture; all interesting orbitals (Figure S3B) are localized on the core and the Gouterman orbitals, not perturbed by other heteroatoms, are in accord with the picture already discussed for porphyrine, with large MCD contributions in correspondence to the Q band, and quite small ones for the B band. In detail, as seen in Table 1D, the MCD spectrum is well accounted for by positive A-terms; important B-terms are calculated in correspondence to the B region but they are opposite and nearly degenerate, so they nearly cancel each other. Notice that aiming to compare MgOESPz and MgOEPz orbitals to evidence sulfur contributions, we maintained the *uudd* conformation also for the MgOEPz complex, despite the fact that it is not the lowest energy one and it possesses lower symmetry than the usual one *udud*. A similar comparison has been conducted in ref 78 with octaethyl pendants, but in that case two different symmetries have been considered for the alkyl and for the thioalkyl cases.

Considering that the MCD spectra were recorded in solution, one cannot exclude the participation of other conformers whose calculated populations depend also on the adopted DFT method, particularly with alkyl and thioalkyl pendants (by the way, BP86/TZVP by the Gaussian package gives similar energy values for *uudd* and *udud* conformers of MgOESPz, the first one with a slightly lower value; considering

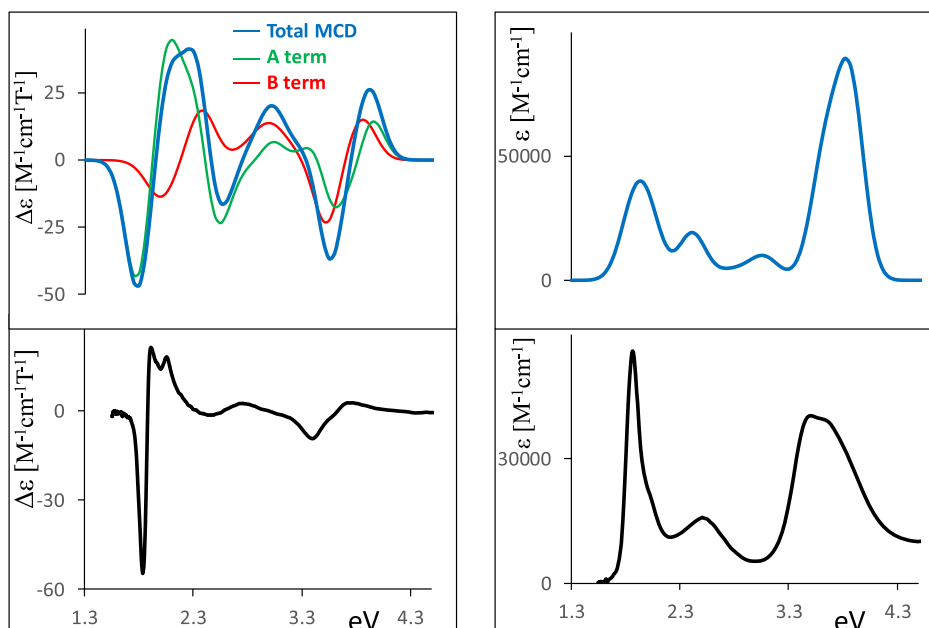


**Figure 6.** Comparison of experimental (black lines) and calculated (colored lines) UV-vis and MCD spectra of CuOESPz.

instead BP86/TZP calculations with the ADF *uudd* conformer is more stable such that the calculated *udud* conformer population is negligible). As an example, we report here both conformers for MgOESPz to analyze the effect on A- and B-terms (see Figure S4). It is interesting to notice that the final result (i.e., A + B) is quite similar in shape for the two cases; only some wavelength shift is observed, which can at least partially explain the band broadness observed for these compounds; the detailed contributions from A and B instead are quite different, the major differences being observed in the high-energy spectroscopic range, where many orbitals interact to give the “bright” transitions. Obviously, the details of the orbital description and band assignment are different in the two cases since sulfur *n* orbitals alternate their orientation in a different way in the two cases, dictating the different symmetry.

**Discussion of an Open-Shell System (CuOESPz).** A similar TDDFT analysis as the one presented above, can be conducted also for open-shell systems,<sup>80–82</sup> and we did it for the CuOESPz complex.  $\alpha$  and  $\beta$  energy levels are reported in Figure 5, where we highlighted Gouterman orbitals 26b1 and 29b2 (in red) and MO derived primarily from the  $d_z^2$  orbital of the central metal  $\beta$  31b2 (unoccupied) and  $\beta$  32a1 and  $\alpha$  and  $\beta$  31a1. The latter orbitals are represented in Figure S5; from performed calculations, metal to ligand transitions present negligible contributions to absorption and MCD spectra, see Table S1 for details.

The resulting calculated MCD and absorption spectra are reported in Figure 6, and give acceptable results as compared with the previously examined closed-shell cases; in particular, transition energies are in good correspondence to the observed bands. The shape of the doublet observed in the Q region, similar to what was observed for the Mg complex, is again explained by a negative A-term (at 2.41 eV = 514 nm), which in this case follows two nearly degenerate positive A-terms, calculated at 1.86 (667 nm) and 2.01 eV (614 nm).

**Coordination Chemistry of [Mn(OESPz)(SH)].** As anticipated in the introduction, the thioethyl porphyrazine Mn(II) complex, MnOESPz, possesses peculiar properties at the nucleophilic metallic center compared to the congener

Mn(II) tetrapyrroles.<sup>55–58</sup> In fact, it promotes the easy removal of halogen atoms from halogenated hydrocarbons, via oxidative addition of the halogen to manganese. Moreover, the Mn(II) thioethyl porphyrazine complex, MnOESPz, reacts also toward weak electrophiles like carbon disulfide to afford the hydrosulfide derivative [Mn(OESPz)(SH)] (Scheme 1).<sup>56</sup> This system deserves particular interest from the biological point of view because transition-metal tetrapyrroles with a hydrosulfide axial ligand mimic the spectral properties of cytochrome P-450 and chloroperoxidase<sup>83</sup> and mono- and polynuclear Mn(III) are of central importance in biological systems such as superoxide dismutase<sup>84,85</sup> and catalase.<sup>86</sup> The coordinating capability of the [Mn(OESPz)(SH)] complex is also investigated by titration with a strong unhindered  $\sigma$ -donor base like 1-methylimidazole (1-mim), observing that 1-mim in chloroform coordinates with manganese giving rise to a [Mn(OESPz)(SH)(1-mim)] complex, while in benzene solution, upon addition of 1-mim, a redox Mn(III)/Mn(II) process occurs leading to the formation of a Mn(II) species.<sup>56</sup> Such titration, previously monitored by UV-vis spectroscopy, is repeated herein (vide infra) following the process via MCD spectroscopy and considering a wider 1-mim concentration range.

The initial complex, [Mn(OESPz)(SH)], is characterized by a square pyramidal geometry and total spin  $S = 2$ .<sup>55–58</sup> Its recorded MCD spectrum (Figure 7A) presents two opposite B-terms associated with  $Q_x$  and  $Q_y$  transitions, with a negative signal at 1.67 eV (742 nm) and a positive signal at 1.82 eV (681 nm), the latter one characterized by an evident shoulder. Moving to higher energy, a weak negative feature and an intense positive one are observed, in correspondence to the absorption peak centered at 2.39 eV (519 nm). The Soret region shows several non-well-defined weak MCD signals, while the UV-vis spectrum shows an intense broad absorption. UV-vis and MCD spectra of the [Mn(OESPz)(SH)] complex is simulated by TDDFT calculations (Figure 7A,B). Overall, the main features of MCD and UV-vis spectra are well reproduced, even if the calculated signals are computed at a slightly higher energy.

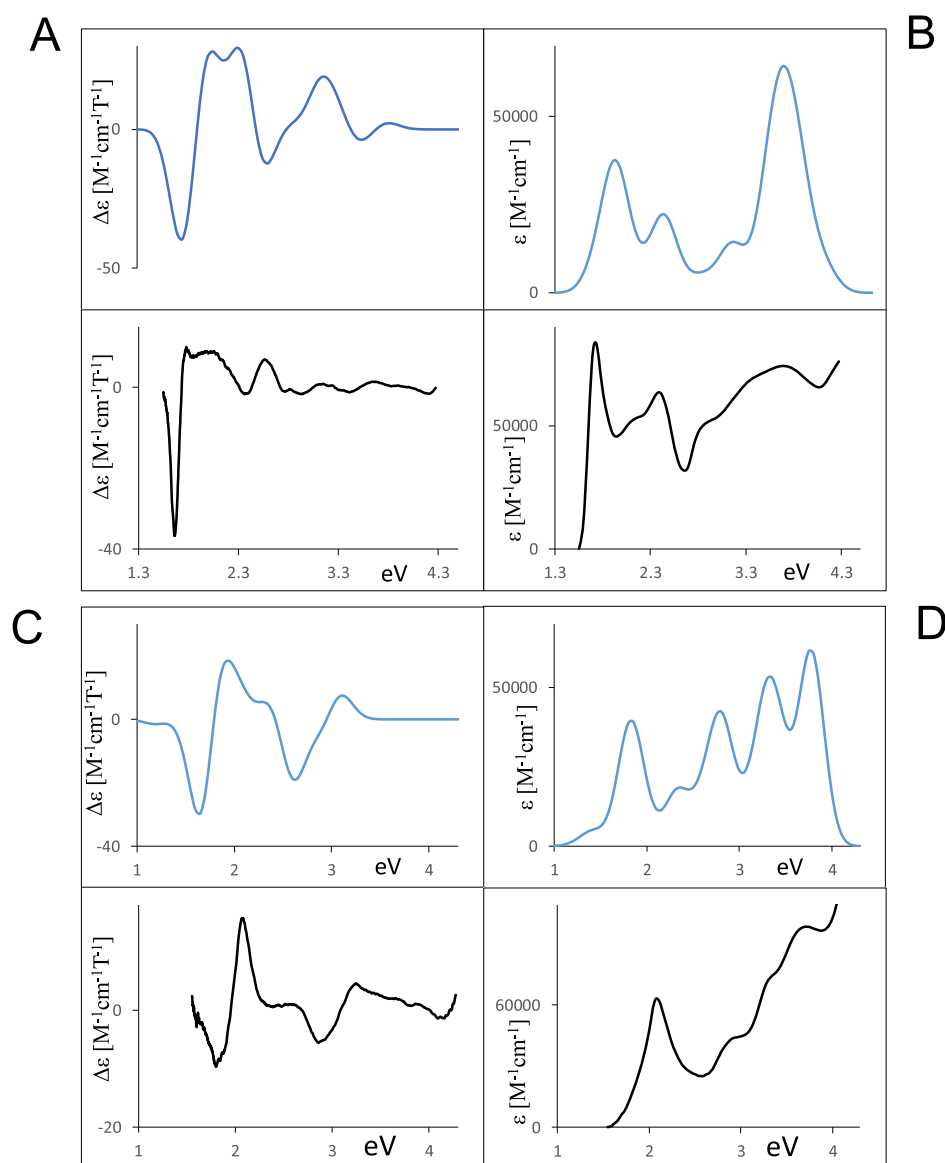


**Figure 7.** Comparison of experimental (black lines) and calculated (blue lines) UV and MCD spectra of the manganese complex. (A) Calculated and experimental MCD spectra of  $[\text{Mn}(\text{OESPz})(\text{SH})]$ . (B) Calculated and experimental UV-vis spectra of  $[\text{Mn}(\text{OESPz})(\text{SH})]$ . (C) Calculated and experimental MCD spectra of  $[\text{Mn}(\text{OESPz})(1\text{-mim})_2]$ . (D) Calculated and experimental UV-vis spectra of  $[\text{Mn}(\text{OESPz})(1\text{-mim})_2]$ .

The  $Q_x$  and  $Q_y$  components can be assigned to transitions from the occupied Gouterman HOMO state to LUMO and LUMO + 1 Gouterman states ( $\alpha 228 \rightarrow 232$  or  $\beta 226 \rightarrow 228$  and  $\alpha 228 \rightarrow 233$  or  $\beta 226 \rightarrow 229$ ), as reported in Table 2. The corresponding orbitals are reported in Figure S6, one may observe that the  $-\text{SH}$  ligand contributes to the LUMO and LUMO + 1 orbitals. The absorption band calculated at 2.39 eV (519 nm) has a  $n \rightarrow \pi^*$  ( $\alpha 223 \rightarrow 232$ ) component involving nitrogen and sulfur atoms of the thioalkyl chains. At a higher energy, we calculate transitions between 3.02 eV (411 nm) and 3.09 eV (401 nm) with some HOMO Gouterman orbital  $\beta 226$  contributions. At 3.45 eV (359 nm), the B band region, a high oscillator strength and a negative B term are calculated in correspondence to a combination of transitions involving the occupied orbitals  $\alpha 217a$ ,  $\beta 215a$  (Gouterman orbitals), and  $\alpha 213a$  with high contributions from the metal and  $-\text{SH}$  ligand. Other orbitals (not shown in Figure S6) are localized on Mn or Mn-SH, however, they do not contribute to “bright” transitions.

Treatment of a dilute (0.012 mM) benzene solution of  $[\text{Mn}(\text{OESPz})(\text{SH})]$  with aliquots of 1-mim in the same solvent, under rigorous anaerobic conditions, leads to isosbestic changes in both the UV-vis and MCD spectra (Figure 8). At relatively high concentrations of the nitrogenous base, limiting spectra indicative of a Mn(II) species was obtained. The observed final MCD spectrum shows a minus-plus signal in the Q region, shifted at a higher energy with respect to the signal of the initial complex  $[\text{Mn}(\text{OESPz})(\text{SH})]$ , in correspondence to the absorption at 2.05 eV (604 nm).

The UV-vis at high energy presents an overlapping of many features, three main components are observed at 2.92, 3.31, and 3.65 eV (425, 375, and 340 nm, respectively). By plotting  $\ln[(\Delta\epsilon_i - \Delta\epsilon)/(\Delta\epsilon - \Delta\epsilon_i)]$  versus  $\ln[1\text{-mim}]$  at various wavelengths<sup>87–89</sup> (see Figure S7), an approximately linear plot is obtained with a slope of  $2 \pm 0.1$ , identifying the reaction as complexation of 2 equiv of the axial ligand 1-mim. The almost isosbestic changes occurring in the visible spectrum may indicate that the possible monoligand intermediate  $[\text{Mn}$

**Table 2. Principal Calculated Transitions Accounting for the Observed Bands: Wavelength (nm), Energy (eV), Oscillator Strength (f), Magnetic Terms A (au) and B (au), and Wavefunctions<sup>a</sup>**

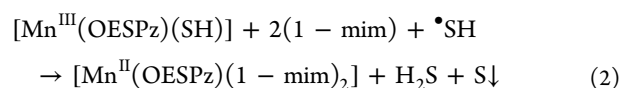
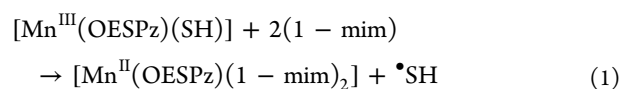
**[Mn(OESPz)(SH)]**

nm	eV	f	$\mathcal{E}$		wavefunction
718	1.73	0.07	-1257.1	Q	$\alpha$ 228a $\rightarrow$ 232a (0.32) $\beta$ 226a $\rightarrow$ 228a (0.20)
661	1.88	0.06	-4395.5		$\alpha$ 225a $\rightarrow$ 233a (0.30) $\alpha$ 229 $\rightarrow$ 234 (0.16)
655	1.89	0.23	4408.1	Q	$\alpha$ 228a $\rightarrow$ 233a (0.44) $\beta$ 226a $\rightarrow$ 229a (0.27)
621	2.00	0.10	631.4		$\alpha$ 229a $\rightarrow$ 234a
558	2.22	0.04	280.9		$\beta$ 219a $\rightarrow$ 228a (0.71) $\alpha$ 223a $\rightarrow$ 232a (0.22)
528	2.35	0.01	-143.5		$\beta$ 219a $\rightarrow$ 229a (0.83) $\alpha$ 223a $\rightarrow$ 233a (0.11)
520	2.39	0.16	1212.4		$\alpha$ 223a $\rightarrow$ 232a (0.73) $\beta$ 219a $\rightarrow$ 228a
498	2.49	0.00	-334.8		$\alpha$ 222a $\rightarrow$ 233a (0.74)
497	2.49	0.04	-619.2		$\alpha$ 223a $\rightarrow$ 233a (0.66) $\beta$ 219a $\rightarrow$ 229a (0.14)
448	2.77	0.00	-170.1		$\beta$ 216a $\rightarrow$ 228a (0.65) $\alpha$ 224a $\rightarrow$ 234a (0.14)
445	2.79	0.01	115.5		$\alpha$ 221a $\rightarrow$ 233a (0.36) $\beta$ 217a $\rightarrow$ 229a (0.31) $\alpha$ 220a $\rightarrow$ 233a (0.26)
430	2.89	0.01	-133.2		$\alpha$ 220a $\rightarrow$ 232a (0.54) $\beta$ 216a $\rightarrow$ 228a (0.16)
426	2.91	0.01	149.5		$\beta$ 216a $\rightarrow$ 229a (0.57) $\alpha$ 220a $\rightarrow$ 233a (0.19)
410	3.02	0.01	18.1	B	$\beta$ 226a $\rightarrow$ 232a (0.41) $\alpha$ 228a $\rightarrow$ 235a (0.14)
410	3.02	0.01	-257.8	B	$\beta$ 226a $\rightarrow$ 232a
406	3.05	0.02	12.7	B	$\beta$ 226a $\rightarrow$ 233a (0.59) $\alpha$ 217a $\rightarrow$ 232a (0.15)
402	3.09	0.04	521.4	B	$\beta$ 225a $\rightarrow$ 233a (0.39) $\beta$ 222a $\rightarrow$ 231a (0.35)
400	3.10	0.02	-214.7		$\beta$ 225a $\rightarrow$ 232a (0.35) $\beta$ 223a $\rightarrow$ 231a (0.25) $\beta$ 220a $\rightarrow$ 230a (0.19)
359	3.45	0.20	-998.1		$\alpha$ 217a $\rightarrow$ 232a (0.24) $\alpha$ 213a $\rightarrow$ 232a (0.22) $\beta$ 215a $\rightarrow$ 228a (0.13)
357	3.47	0.01	-87.4		$\alpha$ 231a $\rightarrow$ 236a (0.45) $\alpha$ 214a $\rightarrow$ 233a (0.23)
356	3.48	0.01	92.7		$\alpha$ 215a $\rightarrow$ 233a
354	3.50	0.02	-63.8		$\beta$ 211a $\rightarrow$ 228a

<sup>a</sup>Gouterman orbitals are written in red.

(OESPz)(SH)(1-mim)] complex is present only in negligible amounts.<sup>89</sup> A similar behavior has been reported for iron(III) porphyrines,<sup>89</sup> porphyrins,<sup>90,91</sup> and protoporphyrins<sup>92</sup> when treated in nonpolar solvents with strong field ligands (imidazoles and pyridines). Taking into account the recently reported inner-sphere reduction mechanism of Fe<sup>III</sup> porphyrin complexes with hydrosulfide ligands,<sup>93</sup> we can hypothesize that the Mn<sup>III</sup>  $\rightarrow$  Mn<sup>II</sup> reduction process occurs with oxidation of HS<sup>-</sup> to elemental sulfur through a two step sequence as reported in eqs 1 and 2. In the first step (eq 1), the reaction proceeds via homolytic cleavage of the Mn<sup>III</sup>-SH bond, releasing a hydrosulfide radical (HS<sup>•</sup>). Subsequently (eq 2) this hydrosulfide radical (SH<sup>•</sup>) reduces another Mn<sup>III</sup>

porphyrine to a Mn<sup>II</sup> complex forming elemental sulfur and releasing a molecule of H<sub>2</sub>S.



This mechanism resembles the biological mechanism of cytochrome *c* reduction by H<sub>2</sub>S<sup>94</sup> and, in general, the interaction with heme centers, where 1-mim can mimic histidine axial coordination.<sup>95,96</sup>

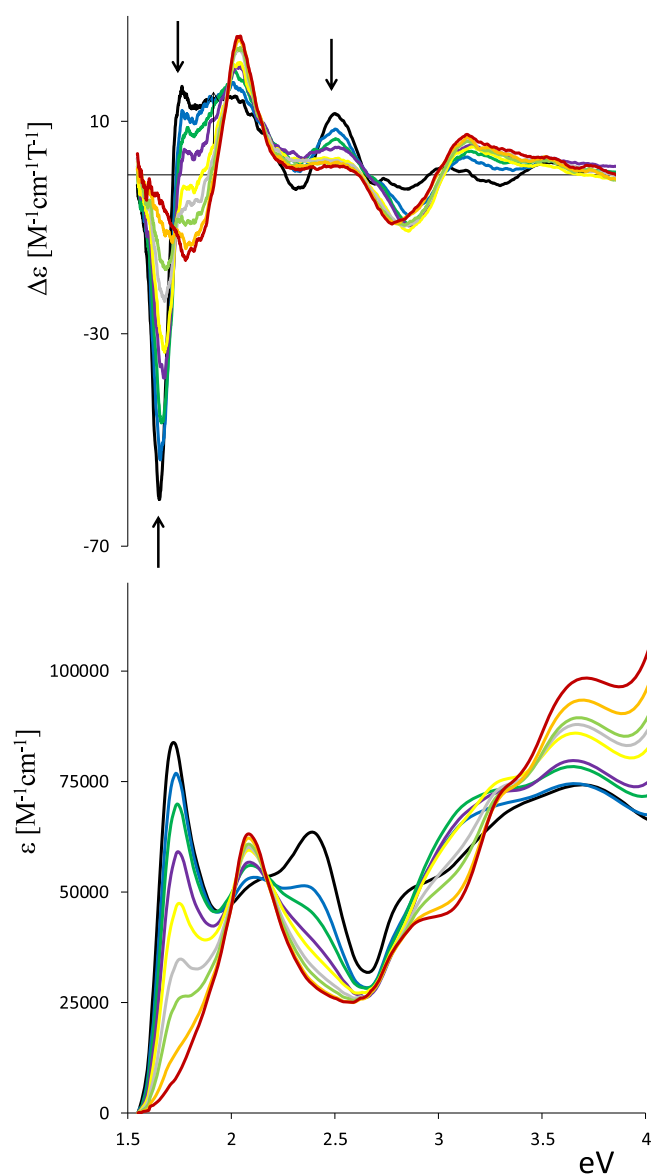


**Figure 8.** Spectroscopic titration of 0.012 mM solution of  $[\text{Mn}(\text{OESPz})(\text{SH})]$  with 1-mim (0–0.294 M) in benzene. Black = no 1-mim and red = highest 1-mim concentration.

To confirm the formation of the hexacoordinate Mn(II) complex  $[\text{Mn}(\text{OESPz})(1\text{-mim})_2]$  suggested by titration analysis, we decided to simulate by TDDFT calculation its UV–vis and MCD spectra. From the analysis reported in ref 58, Mn(II)OESPz has a  $5/2$  spin in the crystal, where it is axially coordinated to two neighbor sulfur atoms, while in solution the tetra-coordinated complex is supposed to have  $S = 3/2$ . For  $[\text{Mn}(\text{OESPz})(1\text{-mim})_2]$ , we considered both spin conditions (as presented in Figure S8). For the  $S = 5/2$  case, the succession of MCD features is correctly represented (i.e., the minus–plus doublet in the Q region and the sign of the B-terms in Q and Soret regions), however, the calculated transition energies are poorly reproduced, in particular the Q band excitation energy is strongly underestimated (Figure 7C,D). The  $S = 3/2$  complex, instead, does not fit the observed features at all (Figure S8). The two possible orientations of the 1-mim groups (parallel and perpendicular) have been considered and show similar calculated spectra. Finally, also  $[\text{Mn}(\text{OESPz})(\text{SH})(1\text{-mim})]$  has been calculated for compar-

ison, as presented in Figure S8. In this case, the calculated absorption spectrum is similar to the recorded one, but the calculated MCD spectrum does not match the experimental data; on the contrary the  $[\text{Mn}(\text{OESPz})(1\text{-mim})_2]$  calculated MCD spectrum well fits the experimental one apart from the energy shift. These findings strongly suggest the formation of the  $[\text{Mn}(\text{OESPz})(1\text{-mim})_2]$  complex upon 1-mim titration of  $[\text{Mn}(\text{OESPz})(\text{SH})]$  in benzene, thus clarifying the nature of the Mn(II) species hypothesized in ref 56.

We repeated the calculations of  $[\text{Mn}(\text{OESPz})(1\text{-mim})_2]$  and  $[\text{Mn}(\text{OESPz})(\text{SH})]$  using the SAOP and B3LYP functional, but we did not obtain any improvement of the representation of the Q transition energies. It is worth recalling here that high-spin open-shell systems are difficult to treat with the linear response formulation of TDDFT;<sup>48,49,97,98</sup> methods such as complete active space self-consistent field (CASSCF)<sup>99</sup> and restricted active space (RAS)<sup>100</sup> wavefunctions should perform better but are beyond the scope of the present work.

## CONCLUSIONS

In conclusion, the analysis of MCD and absorption data supported by TDDFT calculations clearly shows how the red shift observed for thioalkyl-substituted porphyrazine with respect to the analogous alkyl porphyrazine is due to delocalization of the molecular orbitals on sulfur atoms. In particular, sulfur atoms are involved in all bright transitions and, besides contributing to Q and B bands, give rise to the so-called W band.

Substituent thioalkyl chain conformations have an important role in determining molecular symmetry and, since sulfur atoms are heavily involved in optical transitions, A- and B-terms highly depend on the conformation. A test on the lower energy conformers with different symmetry suggests that the resulting MCD pattern A + B is however similar and follows the usual literature interpretation.

Experimental MCD spectra of tetra-coordinated metal OESPz complexes are very similar, with a few slight differences; the calculations herein presented give acceptable results; calculated band energies appear acceptable with no need for an ad hoc wavelength shift, but the B band intensity is overestimated and calculated too high relative to the Q band, which is usually better represented. Of course, simple TDDFT calculations cannot account for band shapes. Despite these limitations, differences in the wavelength of the Q band and of the B band, which are evident when comparing the metal-free, the Ni and, the Mg complexes, are reproduced by calculations (see Figure S9). TDDFT calculations show good correspondence to experimental data also for the open-shell copper complex.

Finally, the use of the MCD technique allows one to accurately monitor titration processes, in particular for the manganese complex, giving clear-cut spectroscopic evidence while varying the base concentration. TDDFT calculations have been performed for the starting complex and the expected product, while the shape of the spectra appears well reproduced, the band position is not correctly calculated. Further studies are needed to better clarify the reduced complex both from the experimental and the calculated point of view. In any case, the comparison of experimental and computed MCD spectra confirms the Mn(III) → Mn(II) redox process that interconverts the  $[\text{Mn}(\text{OESPz})(\text{SH})]$  complex to the  $[\text{Mn}(\text{OESPz})(1\text{-mim})_2]$  species upon 1-mim

treatment in benzene, and the sensitivity of MCD to the spin state suggests the presence of a high spin state ( $S = 5/2$ ).

## ■ ASSOCIATED CONTENT

### SI Supporting Information

The Supporting Information is available free of charge at <https://pubs.acs.org/doi/10.1021/acs.jpbc.0c09277>.

Superposed experimental UV/MCD spectra (Figures S1 and S2); molecular orbitals (Figures S3, S5, and S6); superimposed calculated spectra of conformers *uudd* and *udud* (Figure S4); plots of  $\ln[(\Delta\epsilon_i - \Delta\epsilon)/(\Delta\epsilon - \Delta\epsilon_i)]$  versus  $\ln[1 - \text{mim}]$  at various wavelengths (Figure S7); comparison of calculated spectra of high-spin and low-spin Mn-complexes (Figure S8); and comparison of calculated MCD spectra of ZnOESPz, MgOESPz, and H<sub>2</sub>OESPz complexes and their corresponding experimental spectra (Figure S9) (PDF)

## ■ AUTHOR INFORMATION

### Corresponding Authors

**Sandra Belviso** – Dipartimento di Scienze, Università della Basilicata, 85100 Potenza, Italy; [orcid.org/0000-0002-2997-0129](https://orcid.org/0000-0002-2997-0129); Email: [sandra.belviso@unibas.it](mailto:sandra.belviso@unibas.it)

**Giovanna Longhi** – Dipartimento di Medicina Molecolare e Traslazionale, Università di Brescia, 25123 Brescia, Italy; Research Unit of Brescia, CNR, Istituto Nazionale di Ottica (INO), 25123 Brescia, Italy; [orcid.org/0000-0002-0011-5946](https://orcid.org/0000-0002-0011-5946); Email: [giovanna.longhi@unibs.it](mailto:giovanna.longhi@unibs.it)

### Authors

**Simone Ghidinelli** – Dipartimento di Medicina Molecolare e Traslazionale, Università di Brescia, 25123 Brescia, Italy; [orcid.org/0000-0001-5468-7715](https://orcid.org/0000-0001-5468-7715)

**Sergio Abbate** – Dipartimento di Medicina Molecolare e Traslazionale, Università di Brescia, 25123 Brescia, Italy; Research Unit of Brescia, CNR, Istituto Nazionale di Ottica (INO), 25123 Brescia, Italy; [orcid.org/0000-0001-9359-1214](https://orcid.org/0000-0001-9359-1214)

**Ernesto Santoro** – Dipartimento di Medicina Molecolare e Traslazionale, Università di Brescia, 25123 Brescia, Italy; Dipartimento di Scienze, Università della Basilicata, 85100 Potenza, Italy

Complete contact information is available at: <https://pubs.acs.org/doi/10.1021/acs.jpbc.0c09277>

### Notes

The authors declare no competing financial interest.

## ■ ACKNOWLEDGMENTS

Research was carried out with the support of resources of Big & Open Data Innovation Laboratory (BODaI-Lab), University of Brescia, granted by Fondazione Cariplo and Regione Lombardia and of the Computing Center CINECA (Bologna), Italy. Financial support from the Cariplo Foundation, through Agrofood Lab, University of Brescia for E.S. is acknowledged. The research team in Brescia acknowledges funding from the Italian Ministry of Education, University and Research (MIUR) through the PRIN 2017 program (Project 2017A4XRCA\_003 “Physico-chemical Heuristic Approaches: Nanoscale Theory of Molecular Spectroscopy [PHANTOMS]”). S.B. acknowledges financial support from Università

della Basilicata (R.I.L. 2016 grant) and from MIUR, Project PON RI 2014–2020 BIOFEEDSTOCK.

## ■ REFERENCES

- (1) Walter, M. G.; Rudine, A. B.; Wamser, C. C. Porphyrins and Phthalocyanines in Solar Photovoltaic Cells. *J. Porphyrins Phthalocyanines* **2010**, *14*, 759–792.
- (2) Travkin, V.; Yunin, P.; Stuzhin, P.; Pakhomov, G. Characterization of Vacuum-Deposited Films of Hexachloro-Substituted Subphthalocyanines for Photovoltaic Applications. *Mater. Today: Proc.* **2020**, *20*, 12–15.
- (3) de la Torre, G.; Vazquez, P.; Agullo-Lopez, F.; Torres, T. Role of Structural Factors in the Nonlinear Optical Properties of Phthalocyanines and Related Compounds. *Chem. Rev.* **2004**, *104*, 3723–3750.
- (4) Drobizhev, M.; Makarov, N. S.; Rebane, A.; de la Torre, G.; Torres, T. Strong Two-Photon Absorption in Push–Pull Phthalocyanines: Role of Resonance Enhancement and Permanent Dipole Moment Change upon Excitation. *J. Phys. Chem. C* **2008**, *112*, 848–859.
- (5) Senge, M. O.; Fazekas, M.; Notaras, E. G. A.; Blau, W. J.; Zawadzka, M.; Locos, O. B.; Ni Mhuircheartaigh, E. M. Nonlinear Optical Properties of Porphyrins. *Adv. Mater.* **2007**, *19*, 2737–2774.
- (6) McEwan, K.; Lewis, K.; Yang, G. Y.; Chng, L. L.; Lee, Y. W.; Lau, W. P.; Lai, K. S. Synthesis, Characterization, and Nonlinear Optical Study of Metalloporphyrins. *Adv. Funct. Mater.* **2003**, *13*, 863–867.
- (7) Leznoff, C. C.; Lever, A. B. P., Eds. *Phthalocyanines, Properties and Applications*; VCH: New York, 1989–1996; Vols. 1–4.
- (8) Stuzhin, P. A.; Ercolani, C. In *The Porphyrin Handbook*; Kadish, K. M.; Smith, K. M.; Guillard, R., Eds.; Academic Press: New York, 2003; Vol. 15, p 263.
- (9) Dolphin, D., Ed. *The Porphyrins*; Academic: New York, 1978–1979; Vol. 1–7.
- (10) Forsyth, T. P.; Williams, D. B. G.; Montalban, A. G.; Stern, C. L.; Barrett, A. G. M.; Hoffman, B. M. A Facile and Regioselective Synthesis of Trans-Heterofunctionalized Porphyrazine Derivatives. *J. Org. Chem.* **1998**, *63*, 331–336.
- (11) Lelj, F.; Morelli, G.; Ricciardi, G.; Roviello, A.; Sirigu, A. Discotic Mesomorphism of 2,3,7,8,12,13,17,18-Octakis (Alkyl-Thio) 5,10,15,20 Tetraaza Porphyrin and Its Complexes With Some Divalent Transition Metal Ions Synthesis and Characterization. *Liq. Cryst.* **1992**, *12*, 941–960.
- (12) Belviso, S.; Ricciardi, G.; Lelj, F. Inter-Ring Interactions and Peripheral Tail Effects on the Discotic Mesomorphism of ‘Free-Base’ and Co (ii), Ni (ii) and Cu (ii) Alkenyl (Sulfanyl) Porphyrazines. *J. Mater. Chem.* **2000**, *10*, 297–304.
- (13) Belviso, S.; Amati, M.; De Bonis, M.; Lelj, F. Columnar Discotic Mesophases from Novel Non-Symmetrically Substituted (Octylsulfanyl) Porphyrazines. *Mol. Cryst. Liq. Cryst.* **2008**, *481*, 56–72.
- (14) Belviso, S.; Cammarota, F.; Rossano, R.; Lelj, F. Effect of Polyfluorination on Self-Assembling and Electronic Properties of Thioalkyl-Porphyrazines. *J. Porphyrins Phthalocyanines* **2016**, *20*, 223–233.
- (15) Belviso, S.; Giugliano, A.; Amati, M.; Ricciardi, G.; Lelj, F.; Monsù Scolaro, L. Two-Electron Reduction of Alkyl(sulfanyl)-Porphyrazines: A Route to Free-Base and Peripherally Metallated Asymmetric Porphyrazines. *Dalton Trans.* **2004**, 305–312.
- (16) Nalwa, H. S.; Hanack, M.; Pawlowski, G.; Engel, M. K. Third-Order Nonlinear Optical Properties of Porphyrazine, Phthalocyanine and Naphthalocyanine Germanium Derivatives: Demonstrating the Effect of  $\pi$ -Conjugation Length on Third-Order Optical Nonlinearity of Two-Dimensional Molecules. *Chem. Phys.* **1999**, *245*, 17–26.
- (17) Wen, T. C.; Tsai, C. J. Influence of Azasubstitution on the Nonlinear Absorption in Porphyrazine Derivatives. *Chem. Phys. Lett.* **1999**, *311*, 173–178.
- (18) Donzello, M. P.; Ou, Z.; Dini, D.; Meneghetti, M.; Ercolani, C.; Kadish, K. M. Tetra-2,3-pyrazinoporphyrazines with Externally Appended Pyridine Rings. 2. Metal Complexes of Tetrakis-2,3-[5,6-

di(2-pyridyl)pyrazino]porphyrazine: Linear and Nonlinear Optical Properties and Electrochemical Behavior. *Inorg. Chem.* **2004**, *43*, 8637–8648.

(19) Donzello, M. P.; Ercolani, C.; Stuzhin, P. A. Novel Families of Phthalocyanine-Like Macrocycles—Porphyrazines with Annulated Strongly Electron-Withdrawing 1, 2, 5-Thia/Selenodiazole Rings. *Coord. Chem. Rev.* **2006**, *250*, 1530–1561.

(20) Vagin, S.; Barthel, M.; Dini, D.; Hanack, M. Synthesis and Characterization of (Octaaryl-tetraazaporphyrinato) Indium (III) Complexes for Optical Limiting. *Inorg. Chem.* **2003**, *42*, 2683–2694.

(21) Hanack, M.; Dini, D.; Barthel, M.; Vagin, S. Conjugated Macrocycles as Active Materials in Nonlinear Optical Processes: Optical Limiting Effect with Phthalocyanines and Related Compounds. *Chem. Rec.* **2002**, *2*, 129–148.

(22) Donzello, M. P.; Dini, D.; D'Arcangelo, G.; Ercolani, C.; Zhan, R.; Ou, Z.; Stuzhin, P. A.; Kadish, K. M. Porphyrazines with Annulated Diazepine Rings. 2. Alternative Synthetic Route to Tetrakis-2,3-(5,7-diphenyl-1,4-diazepino)porphyrazines: New Metal Complexes, General Physicochemical Data, Ultraviolet–Visible Linear and Optical Limiting Behavior, and Electrochemical and Spectroelectrochemical Properties. *J. Am. Chem. Soc.* **2003**, *125*, 14190–14204.

(23) Vagin, S.; Yang, G. Y.; Lee, M. K. Y.; Hanack, M. Nonlinear Optical Absorption Studies of New Indium (III) Porphyrazines: Influence of Additional Benzo-Annulation. *Opt. Commun.* **2003**, *228*, 119–125.

(24) Vagin, S.; Hanack, M. Synthesis and Spectroscopic Properties of Non-Symmetrical Benzo-Annulated Porphyrazines and Their Metal Complexes. *Eur. J. Org. Chem.* **2002**, 2859–2865.

(25) Miyoshi, Y.; Fujimoto, T.; Yoshikawa, H.; Matsushita, M. M.; Awaga, K.; Yamada, T.; Ito, H. Photoconductivity and FET Performance of an n-Type Porphyrazine Semiconductor, Tetrakis-(thiadiazole)porphyrazine. *Org. Electron.* **2011**, *12*, 239–243.

(26) Mori, H.; Miyazaki, E.; Osaka, I.; Takimiya, K. Organic Photovoltaics Based on 5-Hexylthiophene-Fused Porphyrazines. *Org. Electron.* **2012**, *13*, 1975–1980.

(27) Belviso, S.; Capasso, A.; Santoro, E.; Najafi, L.; Lelj, F.; Superchi, S.; Casarini, D.; Villani, C.; Spirito, D.; Bellani, S.; Del Rio-Castillo, A. E.; Bonaccorso, F. Thioethyl-Porphyrazine/Nanocarbon Hybrids for Photoinduced Electron Transfer. *Adv. Funct. Mater.* **2018**, *28*, No. 1705418.

(28) Belviso, S.; Santoro, E.; Lelj, F.; Casarini, D.; Villani, C.; Franzini, R.; Superchi, S. Stereochemical Stability and Absolute Configuration of Atropisomeric Thioalkyl-Porphyrazines by Dynamic NMR and HPLC Studies and Computational Analysis of HPLC-ECD Recorded Spectra. *Eur. J. Org. Chem.* **2018**, *2018*, 4029–4037.

(29) Belviso, S.; Amati, M.; Rossano, R.; Crispini, A.; Lelj, F. Non-symmetrical Aryl- and Arylethynyl-Substituted Thioalkyl-Porphyrazines for Optoelectronic Materials: Synthesis, Properties, and Computational Studies. *Dalton Trans.* **2015**, *44*, 2191–2207.

(30) Belviso, S.; Santoro, E.; Penconi, M.; Righetto, S.; Tessore, F. Thioethyl Porphyrazines: Attractive Chromophores for Second-Order Nonlinear Optics and DSSCs. *J. Phys. Chem. C* **2019**, *123*, 13074–13082.

(31) Mason, W. R. *A Practical Guide to Magnetic Circular Dichroism Spectroscopy*; Wiley & Sons, Inc., 2007.

(32) Kobayashi, N.; Nakai, K. Applications of Magnetic Circular Dichroism Spectroscopy to Porphyrins and Phthalocyanines. *Chem Commun.* **2007**, *40*, 4077–4092.

(33) Mack, J.; Stillman, M. J.; Kobayashi, K. Application of MCD Spectroscopy to Porphyrinoids. *Coord. Chem. Rev.* **2007**, *251*, 429–453.

(34) Michl, J. Magnetic Circular Dichroism of Cyclic. $\pi$ -Electron Systems. 1. Algebraic Solution of the Perimeter Model for the A and B Terms of High-Symmetry Systems with a  $(4N + 2)$ -Electron  $[n]$ Annulene Perimeter. *J. Am. Chem. Soc.* **1978**, *100*, 6801–6811.

(35) Michl, J. Magnetic Circular Dichroism of Cyclic. $\pi$ -Electron Systems. 2. Algebraic Solution of the Perimeter Model for the B

Terms of Systems with a  $(4N + 2)$ -Electron  $[n]$ Annulene Perimeter. *J. Am. Chem. Soc.* **1978**, *100*, 6812–6818.

(36) Mack, J.; Stillman, M. J. In *The Porphyrin Handbook*; Kadish, K. M.; Smith, K. M.; Guillard, R., Eds.; Academic Press: New York, 2003; Chapter 103, Vol. 16, pp 43–116.

(37) Piepho, S. B.; Schatz, P. N. *Group Theory in Spectroscopy with Applications to Magnetic Circular Dichroism*; John Wiley & Sons: New York, 1983.

(38) Buckingham, A. D.; Stephens, P. J. Magnetic Optical Activity. *Annu. Rev. Phys. Chem.* **1966**, *17*, 399–432.

(39) Schatz, P. N.; McCaffery, A. J. The Faraday Effect. *Q. Rev., Chem. Soc.* **1969**, *23*, 552–584.

(40) Seth, M.; Ziegler, T. Formulation of Magnetically Perturbed Time-Dependent Density Functional Theory. *J. Chem. Phys.* **2007**, *127*, No. 134108.

(41) Seth, M.; Autschbach, J.; Ziegler, T. Calculation of the B Term of Magnetic Circular Dichroism. A Time-Dependent Density Functional Theory Approach. *J. Chem. Theory Comput.* **2007**, *3*, 434–447.

(42) Seth, M.; Krykunov, M.; Ziegler, T.; Autschbach, J. Application of Magnetically Perturbed Time-Dependent Density Functional Theory to Magnetic Circular Dichroism. II. Calculation of A Terms. *J. Chem. Phys.* **2008**, *128*, No. 234102.

(43) Peralta, G. A.; Seth, M.; Ziegler, T. Magnetic circular dichroism of porphyrins containing M = Ca, Ni, and Zn. A Computational Study Based on Time-Dependent Density Functional Theory. *Inorg. Chem.* **2007**, *46*, 9111–9125.

(44) Štěpánek, P.; Straka, M.; Andrushchenko, V.; Bouř, P. Communication: Fullerene resolution by the magnetic circular dichroism. *J. Chem. Phys.* **2013**, *138*, No. 151103.

(45) Štěpánek, P.; Andrushchenko, V.; Ruud, K.; Bouř, P. Porphyrin Protonation Studied by Magnetic Circular Dichroism. *J. Phys. Chem. A* **2012**, *116*, 778–783.

(46) Solheim, H.; Ruud, K.; Coriani, S.; Norman, P. The A and B Terms of Magnetic Circular Dichroism Revisited. *J. Phys. Chem. A* **2008**, *112*, 9615–9618.

(47) Solheim, H.; Ruud, K.; Coriani, S.; Norman, P. Complex Polarization Propagator Calculations of Magnetic Circular Dichroism Spectra. *J. Chem. Phys.* **2008**, *128*, No. 094103.

(48) Cramer, C. J.; Truhlar, D. G. Density Functional Theory for Transition Metals and Transition Metal Chemistry. *Phys. Chem. Chem. Phys.* **2009**, *11*, 10757–10816.

(49) Neese, F. Prediction of Molecular Properties and Molecular Spectroscopy with Density Functional Theory: From Fundamental Theory to Exchange-Coupling. *Coord. Chem. Rev.* **2009**, *253*, 526–563.

(50) Ziegler, C. J.; Erickson, N. R.; Dahlby, M. R.; Nemykin, V. N. Magnetic Circular Dichroism Spectroscopy of N-Confused Porphyrin and Its Ionized Forms. *J. Phys. Chem. A* **2013**, *117*, 11499–11508.

(51) Doble, S.; Osinski, A. J.; Holland, S. M.; Fisher, J. M.; Geier, G. R., III; Belosludov, R. V.; Ziegler, C. J.; Nemykin, V. N. Magnetic Circular Dichroism of Transition-Metal Complexes of Perfluorophenyl-N-Confused Porphyrins: Inverting Electronic Structure through a Proton. *J. Phys. Chem. A* **2017**, *121*, 3689–3698.

(52) Kobayashi, N.; Nakajima, S.; Osa, T. Spectroscopy, Electrochemistry, and Spectroelectrochemistry of Tetra-tert-Butylated and Octaphenylated Tetraazaporphyrins. *Chem. Lett.* **1992**, *21*, 2415–2418.

(53) Peralta, G. A.; Seth, M.; Zhekova, H.; Ziegler, T. Magnetic Circular Dichroism of Phthalocyanine (M = Mg, Zn) and Tetraazaporphyrin (M = Mg, Zn, Ni) Metal Complexes. A Computational Study Based on Time-Dependent Density Functional Theory. *Inorg. Chem.* **2008**, *47*, 4185–4198.

(54) Ghidinelli, S.; Abbate, S.; Mazzeo, G.; Paoloni, L.; Viola, E.; Ercolani, C.; Donzello, M. P.; Longhi, G. Characterization of Tetrakis(thiadiazole)porphyrazine Metal Complexes by Magnetic Circular Dichroism and Magnetic Circularly Polarized Luminescence. *Chirality* **2020**, *32*, 808–816.

- (55) Ricciardi, G.; Belviso, S.; Lelj, F. The Mn(OESPz) (OESPz<sup>2-</sup> = 2,3,7,8,12,13,17,18-Octakis(ethylsulfanyl)-5,10,15,20-tetraazaporphyrinato Dianion) Complex as an in Situ Regenerative Defluorinating Agent. *Inorg. Chem.* **2000**, *39*, 1618–1620.
- (56) Ricciardi, G.; Bencini, A.; Belviso, S.; Lelj, F. Formation, Crystal Structure and Coordination Chemistry of the [MnIII(oespz)(SH)] [oespz<sup>2-</sup> = 2,3,7,8,12,13,17,18-Octakis(ethylsulfanyl)-5,10,15,20-tetraazaporphyrinato dianion] Complex. *J. Chem. Soc., Dalton Trans.* **1998**, 1985–1991.
- (57) Ricciardi, G.; Bavoso, A.; Bencini, A.; Rosa, A.; Lelj, F.; Bonosi, F. Synthesis, Structure, Magnetic, Spectroscopic and Electrochemical Behaviour of Chloro-Iron(III) and -Manganese(III) Complexes of 2,3,7,8,12,13,17,18-Octakis(ethylsulfanyl)-5,10,15,20-Tetraazaporphyrin. *J. Chem. Soc. Dalton Trans.* **1996**, 2799–2807.
- (58) Ricciardi, G.; Bencini, A.; Bavoso, A.; Rosa, A.; Lelj, F. Crystal Structure of High-Spin (S = 5/2) Manganese(II)2,3,7,8,12,13,17,18-Octakis (ethylsulfanyl)-5,10,15,20-Tetraazaporphyrinate. *J. Chem. Soc., Dalton Trans.* **1996**, 15, 3243–3249.
- (59) Ough, E. A.; Creber, K. A. M.; Stillman, M. J. Electrochemistry and Spectroscopy of Magnesium Octaethyltetraazaporphyrin and Magnesium Octakis(methylthio)tetraazaporphyrin. *Inorg. Chim. Acta* **1996**, *246*, 361–369.
- (60) Ricciardi, G.; Belviso, S.; Lelj, F.; Ristori, S. Synthesis, Spectroscopy and Electrochemistry of Lanthanide Bis-(Ethylsulfanyl) Tetraazaporphyrins. *J. Porphyrins Phthalocyanines* **1998**, *2*, 177–188.
- (61) Ricciardi, G.; Belviso, S.; Giancane, G.; Tafuro, R.; Wagner, T.; Valli, L. Floating Films of a Nonamphiphilic Porphyrine at the Air–Water Interface and LS Multilayer Construction and Optical Characterization. *J. Phys. Chem. B* **2004**, *108*, 7854–7861.
- (62) Belviso, S.; Cavalcante, F.; Lettino, A.; Ragone, P.; Belviso, C. Fly Ash as Raw Material for the Synthesis of Zeolite-Encapsulated Porphyrine and Metallo Porphyrine Tetrapyrrolic Macrocycles. *Microporous Mesoporous Mater.* **2016**, *236*, 228–234.
- (63) te Velde, G.; Bickelhaupt, F. M.; Baerends, E. J.; Fonseca Guerra, C.; van Gisbergen, S. J. A.; Snijders, J. G.; Ziegler, T. Chemistry with ADF. *J. Comput. Chem.* **2001**, *22*, 931–967.
- (64) ADF2018, SCM. *Theoretical Chemistry*; Vrije Universiteit: Amsterdam, The Netherlands, 2018. <http://www.scm.com>.
- (65) Grimme, S.; Antony, J.; Ehrlich, J. A. S.; Krieg, H. A Consistent and Accurate Ab Initio Parametrization of Density Functional Dispersion Correction (DFT-D) for the 94 Elements H–Pu. *J. Chem. Phys.* **2010**, *132*, No. 154104.
- (66) Seth, M.; Ziegler, T. Calculation of Magnetic Circular Dichroism Spectra with Time-Dependent Density Functional Theory. *Adv. Inorg. Chem.* **2010**, *62*, 41–109.
- (67) Schaftenaar, G.; Noordik, J. H. Molden: A Pre- and Post-Processing Program for Molecular and Electronic Structures. *J. Comput.-Aided Mol. Des.* **2000**, *14*, 123–134.
- (68) Wang, F.; Ziegler, T. Excitation Energies of Some d1 Systems Calculated Using Time-Dependent Density Functional Theory: An Implementation of Open-Shell TDDFT Theory for Doublet-Doublet Excitations. *Mol. Phys.* **2004**, *102*, 2585–2595.
- (69) van Lenthe, E.; Ehlers, A.; Baerends, E. J. Geometry Optimizations in the Zero Order Regular Approximation for Relativistic Effects. *J. Chem. Phys.* **1999**, *110*, 8943–8953.
- (70) Guo, L.; Ellis, D. E.; Hoffman, B. M.; Ishikawa, Y. Ligand Substitution Effect on Electronic Structure and Optical Properties of Nickel Porphyrines. *Inorg. Chem.* **1996**, *35*, 5304–5312.
- (71) Belviso, S.; Ricciardi, G.; Lelj, F.; Monsù Scolaro, L.; Bencini, A.; Carbonera, C. Inducing Asymmetry in Free-Base, MnIII, NiII and CuII (Ethylsulfanyl)Porphyrines: Synthetic Aspects and Spectro-Electrochemical Implications. *J. Chem. Soc., Dalton Trans.* **2001**, 7, 1143–1150.
- (72) Infante, I.; Lelj, F. New Investigations of Geometric, Electronic, and Spectroscopic Properties of Tetrapyrrolic Macrocycles by a TD-DFT Approach. Carbon, Nitrogen, and Chalcogen (O, S, Se) Peripheral Substitution Effects on Ni(II) Porphyrinato Complexes. *J. Chem. Theory Comput.* **2007**, *3*, 838–851.
- (73) Weiss, C.; Kobayashi, H.; Gouterman, M. Spectra of porphyrins: Part III. Self-Consistent Molecular Orbital Calculations of Porphyrin and Related Ring Systems. *J. Mol. Spectrosc.* **1965**, *16*, 415–450.
- (74) Baerends, E. J.; Ricciardi, G.; Rosa, A.; van Gisbergen, S. J. A. A DFT/TDDFT Interpretation of the Ground and Excited States of Porphyrin and Porphyrine Complexes. *Coord. Chem. Rev.* **2002**, *230*, 5–27.
- (75) Gouterman, M. In *The Porphyrins*; Dolphin, D., Ed.; Academic Press: New York, 1978; Vol. 3, pp 1–165.
- (76) Michl, J. Magnetic Circular Dichroism of Aromatic Molecules. *Tetrahedron* **1984**, *40*, 3845–3934.
- (77) Moffitt, W. J. Configurational Interaction in Simple Molecular Orbital Theory. *J. Chem. Phys.* **1954**, *22*, 1820–1829.
- (78) Rosa, A.; Ricciardi, G.; Baerends, E. J.; Zimin, M.; Rodgers, M. A. J.; Matsumoto, S.; Ono, N. Structural, Optical, and Photophysical Properties of Nickel(II) Alkylthioporphyrins: Insights from Experimental and DFT/TDDFT Studies. *Inorg. Chem.* **2005**, *44*, 6609–6622.
- (79) Guascito, M. R.; Ricciardi, G.; Rosa, A. Nickel-Macrocyclic Interaction in Nickel(II) Porphyrins and Porphyrines bearing Alkylthio  $\beta$ -Substituents: A Combined DFT and XPS Study. *J. Porphyrins Phthalocyanines* **2017**, *21*, 371–380.
- (80) Mack, J.; Sosa-Vargas, L.; Coles, S. J.; Tizzard, G. J.; Chambrier, I.; Cammidge, A. N.; Cook, M. J.; Kobayashi, N. Synthesis, Characterization, MCD Spectroscopy, and TD-DFT Calculations of Copper-Metalated Nonperipherally Substituted Octaethyl Derivatives of Tetrabenzotriazaporphyrin, Cis- and Trans-Tetrabenzodiazaporphyrin, Tetrabenzomonoazaporphyrin, and Tetrabenzoporphyrin. *Inorg. Chem.* **2012**, *51*, 12820–12833.
- (81) Nevenon, D. E.; Rohde, G. T.; Nemykin, V. N. New Insight into an Old Problem: Analysis, Interpretation, and Theoretical Modeling of the Absorption and Magnetic Circular Dichroism Spectra of Monomeric and Dimeric Zinc Phthalocyanine Cation Radical. *Inorg. Chem.* **2019**, *58*, 14120–14135.
- (82) Zhekova, H. R.; Seth, M.; Ziegler, T. A Magnetic and Electronic Circular Dichroism Study of Azurin, Plastocyanin, Cucumber Basic Protein, and Nitrite Reductase Based on Time-Dependent Density Functional Theory Calculations. *J. Phys. Chem. A* **2010**, *114*, 6308–6321.
- (83) Dawson, J. H.; Sono, M. Cytochrome P-450 and Chloroperoxidase: Thiolate-Ligated Heme Enzymes. Spectroscopic Determination of Their Active Site Structures and Mechanistic Implications of Thiolate Ligation. *Chem. Rev.* **1987**, *87*, 1255–1276.
- (84) Fridovich, I. Superoxide Radical and Superoxide Dismutase. *Annu. Rev. Biochem.* **1995**, *64*, 97.
- (85) Faulkner, K. M.; Liochev, S. I.; Fridovich, I. Stable Mn(III) Porphyrins Mimic Superoxide Dismutase in Vitro and Substitute for it In Vivo. *J. Biol. Chem.* **1994**, *269*, 23471–23476.
- (86) Dismukes, G. C. Manganese Enzymes with Binuclear Active Sites. *Chem. Rev.* **1996**, *96*, 2909–2926.
- (87) Jaffé, H.; Orchin, M. *Theory and Applications of Ultraviolet Spectroscopy*; Wiley: New York, 1962.
- (88) McLees, B.; Caughey, W. Substituted Deuteroporphyrins. V. Structures, Stabilities, and Properties of Nickel (II) Complexes with Axial Ligands. *Biochemistry* **1968**, *7*, 642–652.
- (89) Fitzgerald, J. P.; Haggerty, B. S.; Rheingold, I. A. L.; May, L.; Brewster, G. A. Iron Octaethyltetraazaporphyrins: Synthesis, Characterization, Coordination Chemistry, and Comparisons to Related Iron Porphyrins and Phthalocyanines. *Inorg. Chem.* **1992**, *31*, 2006–2013.
- (90) Collman, J. P. Synthetic Models for the Oxygen-binding Hemoproteins. *Acc. Chem. Res.* **1977**, *10*, 265–272.
- (91) Ellis, P.; Linard, J.; Szymanski, T.; Jones, R.; Budge, J.; Basolo, F. Axial Ligation Constants of Iron (II) and Cobalt (II) "Capped" Porphyrins. *J. Am. Chem. Soc.* **1980**, *102*, 1889–1896.
- (92) Ookubo, S.; Nozawa, T.; Hatano, M. Iron(II) and Iron(III) Low and High Spin Complexes Formed from p-Nitrophenolatoiron-(III) Complex of Protoporphyrin-IX-Dimethylester in the Presence of 1-Methylimidazole: Magnetic Circular Dichroism and <sup>1</sup>H Nuclear

Magnetic Resonance Spectroscopic Studies. *J. Inorg. Biochem.* **1987**, *30*, 45–68.

(93) Mitra, K.; Singha, A.; Dey, A. Mechanism of Reduction of Ferric Porphyrins by Sulfide: Identification of a Low Spin FeIII-SH Intermediate. *Inorg. Chem.* **2017**, *56*, 3916–3925.

(94) Collman, J. P.; Ghosh, S.; Dey, A.; Decreau, R. A. Using a Functional Enzyme Model to Understand the Chemistry Behind Hydrogen Sulfide Induced Hibernation. *Proc. Natl. Acad. Sci. U.S.A.* **2009**, *106*, 22090–22095.

(95) Meiningner, D. J.; Arman, H. D.; Tonzetich, Z. J. Synthesis, Characterization, and Binding Affinity of Hydrosulfide Complexes of Synthetic Iron(II) Porphyrinates. *J. Inorg. Biochem.* **2017**, *167*, 142–149.

(96) Pluth, M. D.; Tonzetich, Z. J. Hydrosulfide Complexes of the Transition Elements: Diverse Roles in Bioinorganic, Cluster, Coordination, and Organometallic Chemistry. *Chem. Soc. Rev.* **2020**, *49*, 4070–4134.

(97) Li, Z.; Liu, W. Critical Assessment of TD-DFT for Excited States of Open-Shell Systems: I. Doublet-Doublet Transitions. *J. Chem. Theory Comput.* **2016**, *12*, 238–260.

(98) Ipatov, A.; Cordova, F.; Doriol, L. J.; Casida, M. E. Excited-state Spin-Contamination in Time-Dependent Density-Functional Theory for Molecules with Open-Shell Ground States. *J. Mol. Struct.: THEOCHEM* **2009**, *914*, 60–73.

(99) Ganyushin, D.; Neese, F. First-Principles Calculations of Magnetic Circular Dichroism Spectra. *J. Chem. Phys.* **2008**, *128*, No. 114117.

(100) Heit, Y. N.; Sergentu, D. C.; Autschbach, J. Magnetic Circular Dichroism Spectra of Transition Metal Complexes Calculated from Restricted Active Space Wavefunctions. *Phys. Chem. Chem. Phys.* **2019**, *21*, 5586–5597.